



Title	Interference effects on light scattering properties of dense colloidal suspensions : a short review
Author(s)	Fujii, Hiroyuki; Na, Hyeonwoo; Nishikawa, Koyata; Kobayashi, Kazumichi; Watanabe, Masao
Citation	Optical Review, 31(3), 299-308 <a href="https://doi.org/10.1007/s10043-024-00887-3">https://doi.org/10.1007/s10043-024-00887-3</a>
Issue Date	2024-06
Doc URL	<a href="http://hdl.handle.net/2115/92592">http://hdl.handle.net/2115/92592</a>
Rights	The version of record of this article, first published in Optical Review, is available online at Publisher ' s website: <a href="http://dx.doi.org/10.1007/s10043-024-00887-3">http://dx.doi.org/10.1007/s10043-024-00887-3</a>
Rights(URL)	<a href="https://creativecommons.org/licenses/by/4.0/">https://creativecommons.org/licenses/by/4.0/</a>
Type	article
File Information	OP31-3_299-308.pdf



[Instructions for use](#)



# Interference effects on light scattering properties of dense colloidal suspensions: a short review

Hiroyuki Fujii<sup>1</sup> · Hyeonwoo Na<sup>1</sup> · Koyata Nishikawa<sup>1</sup> · Kazumichi Kobayashi<sup>1</sup> · Masao Watanabe<sup>1</sup>

Received: 16 January 2024 / Accepted: 30 April 2024 / Published online: 22 May 2024  
© The Author(s) 2024

## Abstract

Near-infrared spectroscopy and imaging using scattered light potentially evaluate the structural properties of the medium, like the average particle size, based on a relation between its structure and light scattering. A qualitative understanding of light scattering is crucial for developing optical imaging techniques. The scattering properties of dense colloidal suspensions have been extensively investigated using the electromagnetic theory (EMT). The colloidal suspensions are widely used in liquid tissue phantoms for optical imaging techniques and are encountered in various fields, such as the food and chemical industries. The interference between electric fields scattered by colloidal particles significantly influences the scattering properties, so-called the interference effects. Despite many efforts since the 1980s, a complete understanding of the interference effects has still not been achieved. The main reason is the complicated dependence of the interference on the optical wavelength, particle size, and so on. This paper briefly reviews numerical and theoretical studies of the interference effect based on the dependent scattering theory, one of the EMTs, and model equations.

**Keywords** Near-infrared spectroscopy and imaging · Light scattering · Interference effect · Dependent scattering theory · Model equations

**Mathematics Subject Classification** 33-04 · 41-04 · 78-04 · 82-04 · 82D15

## 1 Introduction

Near-infrared spectroscopy and imaging (NIRS and NIRI) can evaluate nondestructively chemical components of water-rich dense media, such as biological tissues and agricultural products. NIRS and NIRI are widely used in various application fields, such as biomedical diagnosis [1–3], the food industry [4, 5], and medical pharmacy [6]. On the other hand, NIRS and NIRI using scattered light can potentially evaluate structural properties, such as average particle size and firmness [7–9]. The optical techniques rely on a relation between the medium structure and light scattering.

In the near-infrared wavelength (600–1000 nm), light is strongly scattered by the media, resulting in frequent changes of light directions and spreading a light distribution [10–12]. Moreover, scattering spectra do not have a clear peak, unlike absorption spectra. These facts make it difficult to analyze the light propagation and evaluate the physico-chemical properties of the medium compared to weakly scattering media. For further developments of NIRS and NIRI, a quantitative understanding of light scattering is crucial by accurate evaluations of the scattering properties. As an example of the scattering properties, the reduced scattering coefficient quantifies the scattering event number at unit length and corresponds to the inverse of the photon mean free path at the diffusive regime.

The colloidal suspensions are encountered in numerous fields, such as fat emulsion in medical pharmacy, milk in food science, and slurry in chemical engineering. The materials are also used for a preliminary study of optical technology. The scattering properties are adjustable by changing the volume fraction and the colloidal particle

---

✉ Hiroyuki Fujii  
fujii-hr@eng.hokudai.ac.jp

<sup>1</sup> Division of Mechanical and Space Engineering, Faculty of Engineering, Hokkaido University, Kita 13 Nishi 8, Kita-ku, Sapporo 060-8628, Hokkaido, Japan

diameter [13]. Experimentally, the inverse analysis determines the scattering properties to minimize a difference in light intensity between measurement data and computational results by the radiative transfer theory (RTT) [14–16]. The RTT describes light propagation on a millimeter scale. [3, 17, 18]. On the macroscopic scale, a medium can be considered as a continuous medium with a distribution of optical properties (scattering and absorption properties). Meanwhile, the scattering properties are calculated from the electromagnetic theory (EMT) on a sub-micrometer scale, where a structure size like a particle diameter is comparable to the optical wavelength [19–21]. On the microscopic scale, a medium is regarded as a system consisting of discrete particles in a background continuous medium. The comparison of the inverse analysis with the EMT calculation allows us to perform the validation test for the optical imaging techniques.

There are two kinds of EMTs for colloidal suspensions: the independent and dependent scattering theories (IST and DST). The IST considers no interaction of electric fields scattered by colloidal particles [22, 23]. Meanwhile, the DST treats the interference induced by a superposition of the scattering fields in the far-field [22, 23]. The IST nicely describes experimental results by the inverse analysis at a low volume fraction, approximately less than 5% [24]. At a high volume fraction up to approximately 20%, meanwhile, the DST describes well with experimental results [25, 26]. The DST results are usually smaller than the IST results at a high volume fraction region. The reduction of the scattering properties is so-called the interference effect. The interference effects have been experimentally observed in various systems: polystyrene [27, 28], silica [25], soybean milk [29], technical polymers [7], fat emulsions [30], snow layers [31], and so on, meaning the effects are general phenomena. Although the interference effect has been extensively discussed since the 1980s [7, 21, 25, 27, 28, 30–34], the interference effect has not been fully understood. The main reason is that the interference effect depends on the optical wavelength, particle size distribution, etc., in a complicated way. Moreover, the DST does not explicitly provide the volume fraction dependence of the scattering properties. Recently, we have developed the model equations for the volume fraction dependence of the scattering properties [26]. The model equations allow us to conduct a simple and fast investigation of the interference effects.

This paper briefly reviews numerical and theoretical studies of the interference effect on the scattering properties of dense colloidal suspensions. Although great reviews and textbooks on the interference effect are available [22, 23, 35, 36], we hope this review can help readers find new features of the interference effect.

## 2 Theories and models

### 2.1 Colloidal suspensions

Various colloidal suspensions have been used in examinations of light scattering properties; fat emulsions like Intralipid [19, 20, 24, 30], polystyrene [27, 28], alumina [37], silica [25], and titanium dioxide suspensions [38], soymilk [9, 29], milk [39] and etc. Chemical industrial materials, such as polystyrene and silica systems, can be regarded as monodisperse systems because the size distribution is sufficiently sharp. Then, the monodisperse EMT is applicable. Food materials, including fat emulsions, are polydisperse systems whose size distribution is broad and logarithmic. For such cases, the size polydispersity must be treated in the EMT.

### 2.2 Scattering processes of colloidal suspensions

There are mainly two kinds of electromagnetic scattering processes in colloidal suspensions (many-particle systems) at the near-infrared wavelength: scattering by a single particle and interference between electric fields scattered from colloidal particles at the far-field. The EMT describes the scattering processes on the microscopic scale. The Mie theory describes the former scattering with the size parameter [40]. The size parameter is defined as  $\pi dn_b/\lambda$  with the colloidal particle size  $d$ , the refractive index of the background medium  $n_b$ , and optical wavelength  $\lambda$ . In the current cases of  $d$  in the order of sub-micrometer and  $\lambda$  in the 600–1000 nm range, the size parameter is  $O(1)$ . Hence, applying the Rayleigh theory to single-particle scattering is limited in the current cases. The interference, the latter scattering, depends on the average particle configuration as shown in Fig. 1a. The two scattering processes are dominant over other scattering processes, such as scattering by the solvent molecules and density fluctuation in a solvent medium [11].

We mainly discuss two scattering properties: the scattering coefficient  $\mu_s$  and the reduced scattering coefficient

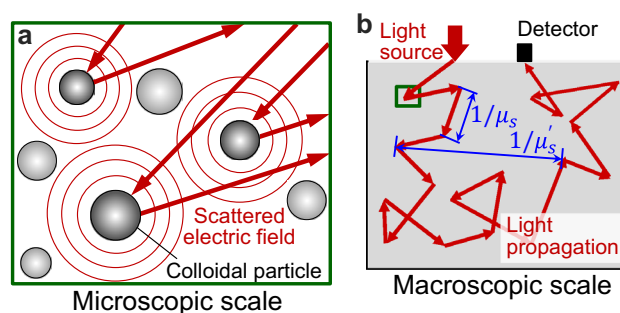


**Fig. 1** Scattering processes in colloidal suspensions on **a** the microscopic and **b** macroscopic scales. The figure **a** is enlarged in the green square of the figure **b**, corresponding to an infinitesimal volume

$\mu'_s$ . The scattering and reduced scattering coefficients quantify the strengths of light scattering per length and correspond to the inverse of the photon mean free paths at ballistic and diffusive regimes of light propagation as shown in Fig. 1b. In the ballistic regime, near the light source, light is less scattered. In the diffusive regime, far from the light source, light can be diffusive because of the multiple scattering of light. The crossover length from the ballistic and diffusive regimes has been evaluated at approximately  $10/(\mu'_s + \mu_a)$  with the absorption coefficient  $\mu_a$  [41, 42].

### 2.3 Independent and dependent scattering theories (IST and DST)

The IST and DST provide formulations of the scattering properties of colloidal suspensions based on the EMT. The term “dependent scattering” is a counterpart of the term “independent scattering”. Although the term “dependent scattering” has been widely used, it has some ambiguity, pointed out by the reference [43]. This paper refers to the IST and DST as theories based on the zeroth-order and first-order expansions of the Foldy-Lax equation (FLE). The FLE is the expansion form of multiple scattering of electric fields and is equivalent to the Maxwell equations [23, 44, 45]. The concept of “multiple scattering of electric fields” is on the microscopic scale, and hence, it is quite different from that of “multiple scattering of light” on the macroscopic scale.

#### 2.3.1 Monodisperse systems

The scattering coefficient is theoretically given by integrating the phase function over the whole solid angle. The monodisperse DST provides the formulation as

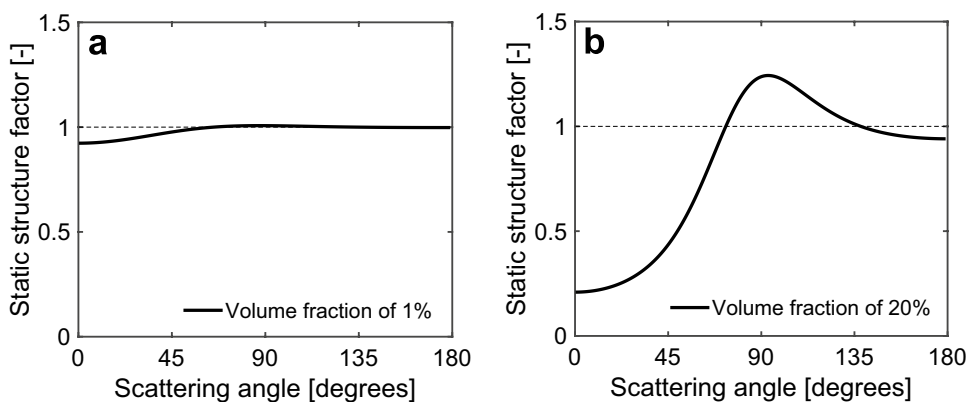
$$\mu_s = 2\pi n_0 \sigma_{s,Mie} \int_0^\pi d\theta \sin \theta \hat{P}_{Mie}(\theta) S_M(\theta). \tag{1}$$

Here, the number density  $n_0$  is given as  $\eta/v_0$ , where  $v_0 = \pi d^3/6$  is the particle volume, and  $\eta$  is the volume fraction of colloidal particles.  $\sigma_{s,Mie}$  and  $\hat{P}_{Mie}$  are the scattering cross section and normalized phase function using the Mie theory [40], and their products are called the form factor. The scattering angle  $\theta$  is set to be equal to a polar angle.  $S_M$  is the static structure factor (SSF) for a monodisperse system.

The SSF is the Fourier transform of the radial distribution function (also called the pair correlation function), representing the local particle configuration [46]. The SSF is averaged over ensembles of equilibrium states and depends on the volume fraction. Therefore, the above DST formula treats the interference by statistically averaged structure of the colloidal systems. The SSF calculation in the DST requires the interaction model between colloidal particles, and the Percus–Yevick (PY) model [47] has been widely used. The PY model treats the hard-sphere interaction and provides the analytical form of the SSF [46]. Although the PY model does not consider solvent molecules, the DST with the PY model describes well measurement data [25, 27, 28]. This fact means that the influences of solvent molecules on the SSF are negligibly small. Figure 2 shows the SSF of the monodisperse PY model at volume fractions of 1% and 20% as a function of the scattering angle.  $S_M = 1$  means no interference, and  $S_M > 1$  and  $S_M < 1$  correspond to the constructive and destructive interference, respectively. At the volume fraction of 1%, the SSF is almost unity for the scattering angles, meaning the weak interference. Meanwhile, at the volume fraction of 20%, the SSF differs from unity, meaning strong interference.

The scattering coefficient of the monodisperse IST is given as  $n_0 \sigma_{s,Mie}$  from the DST formulation (Eq. (1)) by considering  $S_M = 1$  at all the scattering angles. The scattering and reduced scattering coefficients using the IST are linear as a function of

**Fig. 2** Static structure factor (SSF) of the monodisperse PY model at volume fractions of **a** 1% and **b** 20% as a function of the scattering angle at the particle diameter of 300 nm and optical wavelength of 600 nm



the volume fraction. As formulations of the DST and IST for the other scattering properties, please see the reference [25, 27, 28].

### 2.3.2 Polydisperse systems

As a size polydisperse system, we consider a discrete size distribution, whose total number of the diameter classes is  $N_d$ . We denote a particle diameter class by  $\alpha$  or  $\beta$ . The scattering coefficient for the polydisperse DST is given by [48],

$$\mu_s = \int_0^\pi d\theta \int_0^{2\pi} d\phi \sin\theta \sum_{\alpha=1}^{N_d} \sum_{\beta=1}^{N_d} \sqrt{n_\alpha n_\beta} \mathbf{F}_\alpha^{\text{Mie}}(\theta, \phi) \cdot \mathbf{F}_\beta^{\text{Mie}*}(\theta, \phi) S_{\alpha\beta}(\theta). \quad (2)$$

Here,  $\phi$  is the azimuthal angle;  $n_\alpha$  or  $n_\beta$  is the number density for the  $\alpha$ -class or the  $\beta$ -class;  $\mathbf{F}_\alpha^{\text{Mie}}(\theta, \phi)$  is the scattering amplitude vector using the Mie theory [40];  $\mathbf{F}_\beta^{\text{Mie}*}(\theta, \phi)$  is the complex conjugate of  $\mathbf{F}_\beta^{\text{Mie}}(\theta, \phi)$ ; and  $S_{\alpha\beta}(\theta)$  is the partial SSF. The polydisperse PY model [47, 49] calculates the partial SSF. It is noted that L. Tsang's group is a pioneer in developing the polydisperse DST at the remote sensing [23], but the formulation is more general with T-matrix and different from Eq. (2). We can reduce the polydisperse IST by considering  $S_{\alpha\beta}(\theta) = \delta_{\alpha\beta}$  with the Kronecker delta function  $\delta_{\alpha\beta}$ .

### 2.4 Model equations in an exponential form

Although the interference effect has been examined using the DST since the 1980s, a full understanding of the interference effect has not been achieved. The possible reasons are described in the following. First, in the DST, the contributions of the single-particle scattering and interference are coupled, resulting in the difficulty of evaluating the interference contribution separately. Second, the DST calculation requires prior information, such as a particle size distribution. In measurements, such prior information is sometimes unknown, so we cannot employ the DST in that case. Third, the DST has a complicated mathematical formulation based on the summation of the special function (e.g., the Riccati–Bessel function) and the SSF. This fact leads to unveiling the dependence of the interference on the volume fraction, optical wavelength, and so on. To tackle the above challenges, we developed simple model equations for the scattering properties [26].

The model equation for the scattering coefficient  $\mu_{s,M}(\eta, \lambda)$  is given as

$$\mu_{s,M}(\eta, \lambda) = C_{s1}(\lambda)\eta \exp[-C_{s2}(\lambda)\eta]. \quad (3)$$

In the model equation, the interference part is approximated to an exponential form. The coefficient  $C_{s1}(\lambda)$  represents the contribution of the single-particle scattering, regardless of the volume fraction  $\eta$ . The coefficient can be determined theoretically by the IST when we have the prior information,

$$C_{s1}(\lambda) = \mu_{s,IST}(\lambda)/\eta, \quad (4)$$

with the scattering coefficient of the polydisperse IST,  $\mu_{s,IST}(\lambda)$ . Because  $\mu_{s,IST}(\lambda)$  linearly depends on  $\eta$ ,  $C_{s1}(\lambda)$  is independent of  $\eta$ . The coefficient  $C_{s2}(\lambda)$ , referred to as the interference factor, represents the interference contribution independently of  $\eta$ . The interference factor includes the many-body correlations between particles because the PY model for the SSF treats the correlations [50]. We determined a value of  $C_{s2}(\lambda)$  by fitting.

The model equation for the reduced scattering coefficient  $\mu'_{s,M}(\eta, \lambda)$  is given as

$$\mu'_{s,M}(\eta, \lambda) = C_{p1}(\lambda)\eta \exp[-C_{p2}(\lambda)\eta], \quad (5)$$

where the coefficients  $C_{p1}(\lambda)$  and  $C_{p2}(\lambda)$  represent the contributions of the single-particle scattering and interference, respectively, as well as  $C_{s1}(\lambda)$  and  $C_{s2}(\lambda)$ . Theoretical value of  $C_{p1}(\lambda)$  is calculated as

$$C_{p1}(\lambda) = \mu'_{s,IST}(\lambda)/\eta, \quad (6)$$

with the reduced scattering coefficient of the polydisperse IST,  $\mu'_{s,IST}(\lambda)$ . The model equations allow us to investigate the contributions of the single-particle scattering and interference, separately unlike the DST. We summarize the properties of our model equations in Table 1.

### 2.5 Model equations in the Twersky form

Another formula of the model equations has been proposed by Aernouts et al. based on the Twersky theory, one of the DSTs [51]. The correction factor to account for the dependent scattering, the so-called Twersky factor, is given as

$$W(\eta, p) = \frac{(1 - \eta)^{p+1}}{[1 + \eta(p - 1)]^{p-1}}, \quad (7)$$

where  $p$  is the exponent and is theoretically given as integers for geometrical shapes: 1 for plate, 2 for cylinder, and 3 for sphere [52, 53]. Meanwhile, in the model equations, the exponent  $p$  is regarded as a fitting parameter (usually a real number) and depends on the optical wavelength. The model equation for the scattering coefficient is obtained by multiplying the IST result with the Twersky factor,

$$\mu_{s,T}(\eta, \lambda) = \mu_{s,IST}(\eta, \lambda)W(\eta, p(\lambda)). \quad (8)$$

**Table 1** Model equations in the exponential form, developed by us [26] for the scattering and reduced scattering coefficients,  $\mu_s$  and  $\mu'_s$ , in two cases where the prior information (e.g., a particle size distribution) is known to calculate the IST or not

Quantity	Model	Fitting parameter	Note
$\mu_s$	Eq. (3)	$C_{s2}$	$C_{s1}$ can be calculated by the IST with the prior information Direct $\mu_s$ analysis is possible
		$C_{s1}, C_{s2}$	The prior information is not needed Direct $\mu_s$ analysis is possible
$\mu'_s$	Eq. (5)	$C_{p2}$	$C_{p1}$ can be calculated by the IST with the prior information Direct $\mu'_s$ analysis is possible
		$C_{p1}, C_{p2}$	The prior information is not needed Direct $\mu'_s$ analysis is possible

The model equation for the reduced scattering coefficient based on the Twersky factor has two kinds of forms in the following. Aernouts and coworkers developed the model equation as [51]

$$\begin{aligned} \mu'_{s,Ae}(\eta, \lambda) &= \mu_{s,T}(\eta, \lambda) [1 - g_L(\eta, \lambda)] \\ &= \mu_{s,IST}(\eta, \lambda) W(\eta, p) [1 - g_{IST}(\eta, \lambda) - k(\lambda)\eta]. \end{aligned} \tag{9}$$

Here,  $g_L = g_{IST} + k\eta$  is the linear model equation for the anisotropy factor with the volume fraction, and  $k$  is another fitting parameter representing the interference and depends on the wavelength. The anisotropy factor characterizes the scattering anisotropy and ranges from -1 to 1. The above model equation needs to evaluate the fitting parameters  $p$  and  $k$  from the volume fraction dependence of the scattering coefficient and anisotropy factor before applying the results of the reduced scattering coefficient. These prior procedures are not always applicable because some measurements evaluate only the reduced scattering coefficient. To solve the challenge, they examined the wavelength dependence of the parameters [51]. However, the wavelength dependence for other systems is still unclear.

Recently, Pilvar and coworkers proposed the model equation for the reduced scattering coefficient [54], to solve the challenge,

$$\mu'_{s, Pi} = \mu'_{s,IST}(\eta, \lambda) W(\eta, q(\lambda)). \tag{10}$$

The parameter  $q$  can be directly determined from the results of the reduced scattering coefficient, so the  $q$  value is generally different from the  $p$  value of Eq. (9). This model equation seems to omit the high order term,  $\mu_{s,IST} Wk\eta$ , in  $\mu'_{s,Ae}$  (Eq. (9)). They reported that the model equation describes measurement data of lipoproteins in blood [54]. We summarize the properties of the model equations in the Twersky form in Table 2.

This paper examined the DST results using the model equations in the Twersky and exponential forms. Because we can calculate the anisotropy factor using the DST, we can compare the three model equations for the reduced scattering coefficient: Eqs. (9), (10), and (5).

### 3 Numerical results

#### 3.1 Results of the DST and IST

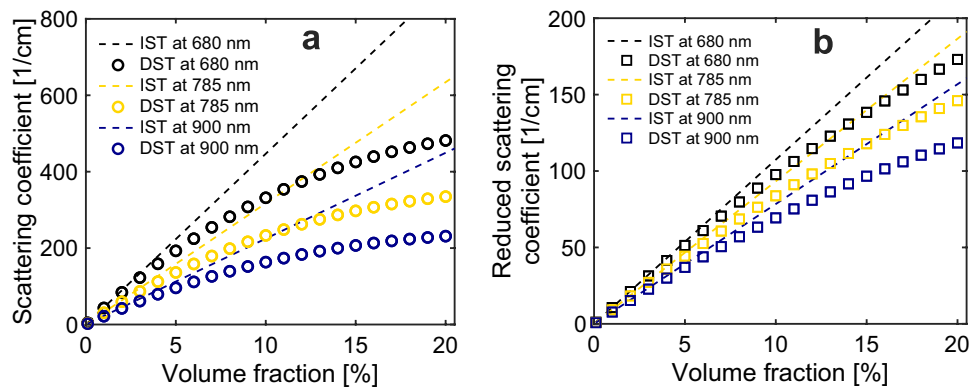
We calculated the scattering properties using the polydisperse DST and IST at different volume fractions from 0.1% to 20% and wavelengths from 600 to 980 nm. We used the particle size distribution of Intralipid-20% (fat emulsion) based on the reference [55]. The average particle diameter is 214.3 nm, and  $N_d$  is 34. The numerical calculation considers the wavelength-dependent refractive indices for the colloidal particle and water by the Cauchy dispersion equation.

**Table 2** Model equations in the Twersky form

Quantity	Model	Fitting parameter	Note
$\mu_s$	Eq. (8)	$p$	IST calculation is needed
	by Aernouts et al. [51]		Direct $\mu_s$ analysis is possible
$\mu'_s$	Eq. (9)	$p, k$	IST calculation is needed
	by Aernouts et al. [51]		Analysis for $\mu_s$ and $g$ is needed
	Eq. (10)	$q$	IST calculation is needed
	by Pilvar et al. [54]		Direct $\mu'_s$ analysis is possible



**Fig. 3** Volume fraction dependence of the scattering coefficients using the DST (Eq. (2)) and IST at different optical wavelengths of 680, 785, and 900 nm: **a** scattering coefficients  $\mu_s$  and **b** reduced scattering coefficients  $\mu'_s$



Although not shown here, our previous study [26] demonstrated that the polydisperse DST results nicely agree with the measurement data by G. Zaccanti and coworkers [30].

Figure 3 shows that as the volume fraction increases, all the results become significant because of the increase in the scatterer number. At a low volume fraction region of approximately less than 5%, the IST results are similar to the DST results. Meanwhile, at the high volume fraction region, the DST results are smaller than the IST results, meaning a reduction of scattering strength by destructive interference. Although not shown here, the anisotropy factor also decreases at the high volume fraction region. These reductions in the scattering coefficients are called the interference effect.

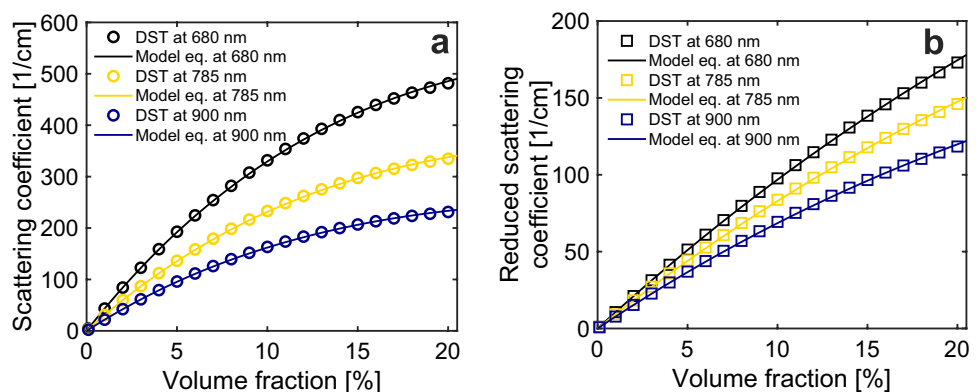
At a long wavelength, the scattering coefficients become smaller. This result is roughly explained in terms of the size parameter; the long wavelength corresponds to the small particle size. A minimum volume fraction where the IST results differ from the DST results seems not to depend on the wavelength strongly. In other words, we did not observe a strong wavelength dependence on the interference effect. The wavelength dependence of the scattering coefficients is mainly ascribed to the single-particle scattering.

### 3.2 Examinations by the model equations

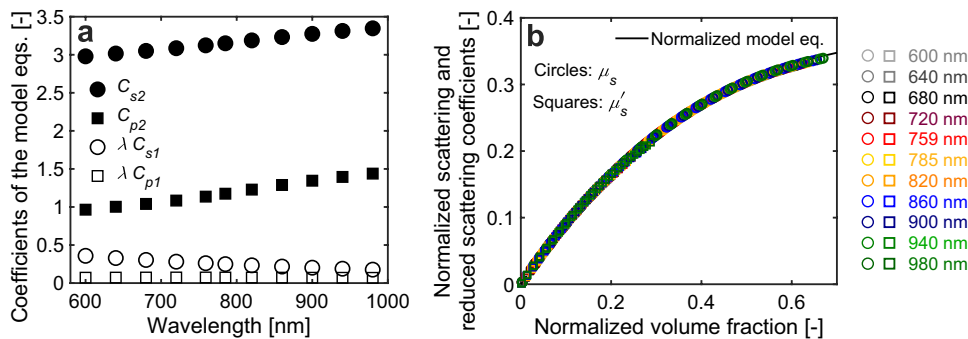
We investigated the DST results using the model equations in the exponential form (Eqs. (3) and (5)) developed by us, as shown in Fig. 4. Here, the coefficients of  $C_{s1}$  and  $C_{p1}$  (single-particle contribution) are calculated by the IST (Eqs. (4) and (6)), while the coefficients of  $C_{s2}$  and  $C_{p2}$  are determined by fitting. We preliminarily confirmed that when  $C_{s1}$  and  $C_{p1}$  are fitting parameters, the evaluated values of  $C_{s1}$  and  $C_{p1}$  are almost the same as the theoretical values. The model equations describe the DST results well at all the wavelengths in the  $R$ -squared values from 0.995 to 0.999.

Figure 5a shows the wavelength dependence of the coefficients in the model equations. Here,  $C_{s1}$  and  $C_{p1}$  are normalized by the inverse wavelength  $1/\lambda$  to be dimensionless as well as  $C_{s2}$  and  $C_{p2}$ .  $\lambda C_{s1}$  and  $\lambda C_{p1}$  are almost constant for the wavelength (especially in  $\lambda C_{p1}$ ), meaning the wavelength dependence of the coefficients is in the form of  $1/\lambda$ . Meanwhile,  $C_{s2}$  and  $C_{p2}$  are almost linearly proportional to the wavelength and their slope values are positive. Hence, the interference effects are enhanced at longer wavelengths, although the enhancement is not so strong compared with the single-particle scattering.

**Fig. 4** Investigations of the DST results using the model equations in the exponential form (Eqs. (3) and (5)) developed by us. Other details are the same as in Fig. 3



**Fig. 5 a** Coefficients of the model equations in the exponential form.  $C_{s1}$  and  $C_{p1}$  are normalized by the inverse of the optical wavelength  $\lambda$  to be dimensionless. **b** Dimensionless analysis of the DST results. The scattering coefficients and volume fraction are normalized by the coefficients of the model equations. Colors represent the wavelengths



The positive values of  $C_{s2}$  and  $C_{p2}$  mean the negative exponential function to the volume fraction works in the scattering coefficients. The negative exponential function reflects the main contribution of the destructive interference rather than the constructive interference. Because the interference relates to the structural properties, such as the average diameter and particle interaction,  $C_{s2}$  and  $C_{p2}$  include the structure information.

We can perform the dimensionless analysis of the scattering coefficients using the model equations in the following. We can consider the normalized forms of the model equations using the two coefficients for each scattering coefficient

$$\hat{\mu}_{s,M} = \hat{\eta} \exp(-\hat{\eta}), \quad \hat{\mu}_{s,M} = \mu_{s,M} C_{s2} / C_{s1}, \quad \hat{\eta} = C_{s2} \eta, \tag{11}$$

$$\hat{\mu}'_{s,M} = \hat{\eta} \exp(-\hat{\eta}), \quad \hat{\mu}'_{s,M} = \mu'_{s,M} C_{p2} / C_{p1}, \quad \hat{\eta} = C_{p2} \eta. \tag{12}$$

The normalized forms suggest that when the DST results at different wavelengths are normalized in the above way, they would coincide on the single curve  $\hat{\eta} \exp(-\hat{\eta})$ , independently of the wavelengths. Figure 5b shows the nice coincidence of the results on the single curve, implying the general feature of the interference, regardless of the wavelengths. The same normalized forms in both scattering coefficients suggest the same scattering mechanism in both coefficients. Although not shown here, we confirmed the nice coincidences of the anisotropy factors at different wavelengths by the dimensionless analysis [26]. It is a future work whether our model equations can be applied to other dense systems.

We investigated the DST results using the model equations in the Twersky form. Figure 6a shows that the model equation for the scattering coefficient (Eq. (8)) nicely describes the DST results as well as ours (Eq. (3)). This result means that the Twersky factor (Eq. (7)) describes well the interference in the scattering coefficient. Figure 6b compares the model equations for the reduced scattering coefficient (Eqs. (9) and (10)). The model equation by

Aernouts et al. agrees well with the DST results. Despite the accuracy, the equation requires the prior analysis for the scattering coefficient and anisotropy factor. Although not shown here, the fitting parameters  $k$  in the anisotropy factor were prior evaluated from the DST results in addition to the evaluation of the parameter  $p$  in the scattering coefficient. Meanwhile, the model equation by Pilvar et al. can directly analyze data of the reduced scattering coefficient. However, this model equation does not describe well the DST results, although it describes well measurement data of lipoproteins in blood [54]. This result suggests that the application of the Twersky factor to the reduced scattering coefficient seems to be limited. The applicability of the Twersky factor should be examined in future work.

It is noted that dimensionless analysis using the model equations in the Twersky form is more difficult than our model equations because of the difficulty in finding the normalization factors of the scattering coefficients and volume fraction.

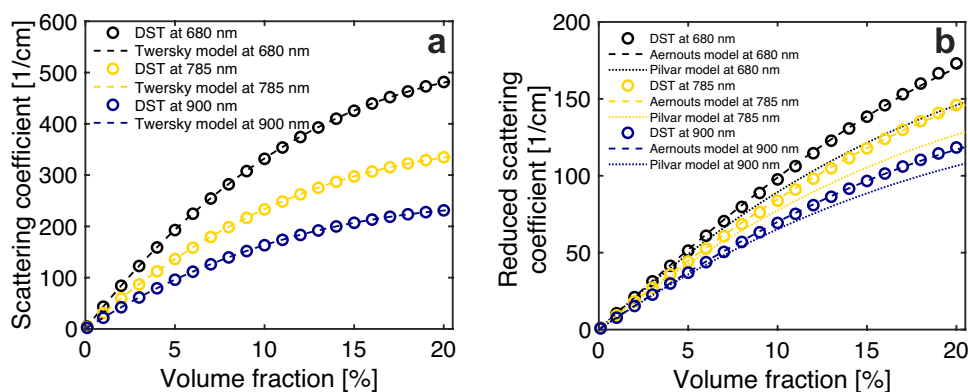
### 4 Numerical studies of the interference effect on light propagation

This paper focuses on the interference effect on the scattering coefficients so far. Meanwhile, the interference influences light propagation as well. This section briefly discusses numerical studies of the interference effect on light propagation and related phenomena.

The interference effect on light propagation has been numerically studied using the radiative transfer theory (RTT) combined with the DST in snow layers [21, 23, 31], and colloidal suspensions [48, 56]. The RTT describes light propagation on a millimeter scale in terms of light intensity and mainly has the radiative transfer and photon diffusion equations [17]. The combined model uses the scattering properties calculated from the DST in the calculation of light propagation. Numerical studies have shown strong interference effects on the light intensity on the macroscopic scale. This fact suggests the significance of the interference



**Fig. 6** Investigations of the DST results using the model equations in the Twersky form for **a** the scattering coefficient (Eq. (7)) and **b** the reduced scattering coefficient (Eqs. (9) and (10)) by Aernouts et al. and Pilvar et al., respectively. Other details are the same as in Fig. 3



effects in static light scattering techniques like NIRS. To examine data on the light intensity, we have developed the model equation for the peak time of the temporal profile of the light intensity [26].

Diffusing-wave spectroscopy, also called diffuse correlation spectroscopy, extends the dynamic light scattering method to turbid media like dense colloidal suspensions [57, 58]. By measuring the light intensity fluctuation, this technique evaluates transport properties of the media, such as short-time self-diffusion coefficient [27, 28], elastic modulus [59], and blood flow rate [60]. This technique requires modeling of light scattering, light propagation, and particle transport. Fraden et al. and Rojas et al. have applied the DST in this technique, implying the significance of the interference effect on the light intensity fluctuation [27, 28].

Photoacoustic imaging (PAI), also called optoacoustic imaging, can evaluate chemical components for biological tissues and foods, *e.g.*, hemoglobin concentration, better than pure optical imaging [10, 12, 61, 62]. Among various PAIs, quantitative PAI is still growing, which aims for the quantitative evaluation deeply inside the media by introducing a model of initial photoacoustic pressure [63–67]. Photoacoustic pressure is generated via several physicochemical processes: laser irradiation, light propagation, light absorption, conversion from optical energy to thermal energy, thermal expansion, etc. We have developed the initial pressure model using the DST [68] and showed the strong interference effect on the initial pressure generated inside media.

## 5 Conclusions

Using the DST and model equations, we briefly discuss numerical studies of the interference effect on the scattering properties. Our model equations have the following five advantages.

- 1) Analytical expression (Fig. 4): the equations describe the volume fraction dependence of the scattering coefficients based on the elementary functions.
- 2) Evaluations of the contributions of single-particle scattering and interference (Fig. 5a): the equations can evaluate the two contributions separately as single effective parameters.
- 3) Fast calculations: the calculations of the model equations take within a few seconds in a condition where the DST calculations take a few days.
- 4) Versatility: the model equations analyze the experimental results without prior information, such as a particle size distribution, while the DST requires the information.
- 5) Dimensionless analysis (Fig. 5b): the model equations enable the performing of the dimensionless analysis to find general features of the scattering properties, independently of optical wavelength and so on.

These advantages help us understand the interference effect, which encounters dense systems.

**Acknowledgements** The first author (H.F.) would like to thank Dr. Y. Hoshi and Dr. S. Okawa (Hamamatsu University School of Medicine), Dr. Y. Yamada (University of Electro-Communications), and Dr. G. Nishimura (Hokkaido University) for their continuous and fruitful comments from the experimental and application point of view since the author worked as a postdoctoral researcher in Tokyo Metropolitan Institute of Medical Science. The authors would like to appreciate the continuous research support from students at Hokkaido University (from K. Hattori in 2014–2016 to H. Kotera and J. Yi currently). H.F. acknowledges financial support from the Konica Minolta Imaging Science Encouragement Award, Grant-in-Aid for Scientific Research (22KK0243, 21H05577) of the Japan Society for the Promotion of Science, KAKENHI, and the Nakatani Foundation.

**Data availability** Data underlying the results presented in this paper are not publicly available at this time but may be obtained from the authors upon reasonable request.

## Declarations

**Conflict of interest** The authors declare that they have no conflict of interest.

**Open Access** This article is licensed under a Creative Commons Attribution 4.0 International License, which permits use, sharing, adaptation, distribution and reproduction in any medium or format, as long as you give appropriate credit to the original author(s) and the source, provide a link to the Creative Commons licence, and indicate if changes were made. The images or other third party material in this article are included in the article's Creative Commons licence, unless indicated otherwise in a credit line to the material. If material is not included in the article's Creative Commons licence and your intended use is not permitted by statutory regulation or exceeds the permitted use, you will need to obtain permission directly from the copyright holder. To view a copy of this licence, visit <http://creativecommons.org/licenses/by/4.0/>.

## References

- Okawa, S., Hoshi, Y., Yamada, Y.: Biomed. Opt. Express **2**(12), 3334 (2011). <https://doi.org/10.1364/BOE.2.003334>
- Hoshi, Y., Yamada, Y.: J. Biomed. Opt. **21**(9), 091312–1 (2016). <https://doi.org/10.1117/1.JBO.21.9.091312>
- Yamada, Y., Suzuki, H., Yamashita, Y.: Appl. Sci. **9**, 1127–1 (2019). <https://doi.org/10.3390/app9061127>
- Tsuchikawa, S., Ma, T., Inagaki, T.: Anal. Sci. **38**(4), 635 (2022). <https://doi.org/10.1007/s44211-022-00106-6>
- Prieto, N., Pawluczyk, O., Dugan, M.E.R., Aalhus, J.L.: Appl. Spectrosc. **71**(7), 1403 (2017). <https://doi.org/10.1177/0003702817709299>
- Lee, J., Duy, P.K., Yoon, J., Chung, H.: Analyst **139**(12), 3179 (2014). <https://doi.org/10.1039/c3an01904g>
- Bressel, L., Hass, R., Reich, O.: J. Quant. Spectrosc. Radiat. Transfer **126**, 122 (2013). <https://doi.org/10.1016/j.jqsrt.2012.11.031>
- Qin, J., Lu, R.: Postharvest Biol. Technol. **49**(3), 355 (2008). <https://doi.org/10.1016/j.postharvbio.2008.03.010>
- Saito, Y., Suzuki, T., Kondo, N.: Infrared Phys. Technol. **123**, 104149 (2022). <https://doi.org/10.1016/j.infrared.2022.104149>
- Ntziachristos, V.: Nat. Methods **7**(8), 603 (2010). <https://doi.org/10.1038/nmeth.1483>
- Tuchin, V.V.: Tissue optics : light scattering methods and instruments for medical diagnosis (SPIE Press,)(2015)
- Wang, L.V., Wu, H.: Biomedical Optics: Principles and Imaging (John Wiley & Sons, Ltd,)(2009)
- Pogue, B.W., Patterson, M.S.: J. Biomed. Opt. **11**(4), 041102–1 (2006). <https://doi.org/10.1117/1.2335429>
- Hoshi, Y., Tanikawa, Y., Okada, E., Kawaguchi, H., Nemoto, M., Shimizu, K., Kodama, T., Watanabe, M.: Scient. Rep. **9**, 9165–1 (2019). <https://doi.org/10.1038/s41598-019-45736-5>
- Bashkatov, A.N., Genina, E.A., Tuchin, V.V.: J. Innov. Opt. Health Sci. **4**(1), 9 (2011). <https://doi.org/10.1142/S1793545811001319>
- Friebel, M., Roggan, A., Müller, G., Meinke, M.: J. Biomed. Opt. **11**(3), 034021–1 (2006). <https://doi.org/10.1117/1.2203659>
- Chandrasekhar, S.: Radiative Transfer (Dover,)(1960)
- Long, F., Li, F., Intes, X., Kotha, S.P.: J. Biomed. Opt. **21**(3), 036003 (2016). <https://doi.org/10.1117/1.JBO.21.3.036003>
- Wen, X., Tuchin, V.V., Luo, Q., Zhu, D.: Phys. Med. Biol. **54**, 6917 (2009). <https://doi.org/10.1088/0031-9155/54/22/011>
- Foschum, F., Kienle, A.: J. Biomed. Opt. **18**(8), 085002 (2013). <https://doi.org/10.1117/1.JBO.18.8.085002>
- Chang, W., Ding, K.H., Tsang, L., Xu, X.: IEEE Trans. Geosci. Remote Sens. **54**(6), 3637 (2016). <https://doi.org/10.1109/TGRS.2016.2522438>
- Tsang, L., Kong, J.A., Ding, K.H.: Scattering of Electromagnetic Waves: Theories and Applications (John Wiley & Sons, Ltd,)(2000)
- Tsang, L., Kong, J.A., Ding, K.H., Ao, C.O.: Scattering of Electromagnetic Waves: Numerical Simulations (John Wiley & Sons, Ltd,)(2001)
- van Staveren, H.J., Moes, C.J.M., van Marie, J., Prah, S.A., van Gemert, M.J.C.: Appl. Opt. **30**(31), 4507 (1991). <https://doi.org/10.1364/AO.30.004507>
- Nguyen, V.D., Faber, D.J., van der Pol, E., van Leeuwen, T.G., Kalkman, J.: Opt. Express **21**(24), 29145 (2013). <https://doi.org/10.1364/OE.21.029145>
- Fujii, H., Ueno, M., Inoue, Y., Aoki, T., Kobayashi, K., Watanabe, M.: Opt. Express **30**(3), 3538 (2022). <https://doi.org/10.1364/OE.447334>
- Rojas-Ochoa, L.F., Romer, S., Scheffold, F., Schurtenberger, P.: Phys. Rev. E **65**(051403), 1 (2002). <https://doi.org/10.1103/PhysRevE.65.051403>
- Fraden, S., Maret, G.: Phys. Rev. Lett. **65**(4), 512 (1990). <https://doi.org/10.1103/PhysRevLett.65.512>
- Ringgenberg, E., Corredig, M., Alexander, M.: Food Biophys. **7**, 244 (2012). <https://doi.org/10.1007/s11483-012-9263-2>
- Zaccanti, G., Bianco, S.D., Martelli, F.: Appl. Opt. **42**(19), 4023 (2003). <https://doi.org/10.1364/ao.42.004023>
- Tsang, L., Kong, J.A., Electromag, J.: Waves Appl. **6**(3), 265 (1992). <https://doi.org/10.1163/156939392X01156>
- Cartigny, J.D., Yamada, Y., Tien, C.L.: J. Heat Transfer **108**, 608 (1986). <https://doi.org/10.1115/1.3246979>
- Yamada, Y., Cartigny, J.D., Tien, C.L.: J. Heat Transfer **108**, 614 (1986). <https://doi.org/10.1115/1.3246980>
- Fujii, H., Nishikawa, K., Na, H., Inoue, Y., Kobayashi, K., Watanabe, M.: Infrared Phys. Technol. **132**, 104753 (2023). <https://doi.org/10.1016/j.infrared.2023.104753>
- Tien, C.L.: J. Heat Transfer **110**(4), 1230 (1988). <https://doi.org/10.1115/1.3250623>
- Wang, B.X., Zhao, C.Y.: Annu. Rev. Heat Transf. **23**(1), 231 (2020). <https://doi.org/10.1615/AnnualRevHeatTransfer.2020.31978>
- Said, Z., Saidur, R., Rahim, N.A.: Int. Commun. Heat Mass Transfer **59**, 46 (2014). <https://doi.org/10.1016/j.icheatmasstransfer.2014.10.010>
- Moreira, J., Serrano, B., Ortiz, A., Lasa, H.D.: Ind. Eng. Chem. Res. **49**, 10524 (2010). <https://doi.org/10.1021/ie100374f>
- Zhao, Z., Corredig, M.: Food Hydrocoll. **60**, 445 (2016). <https://doi.org/10.1016/j.foodhyd.2016.04.016>
- Bohren, C.F., Huffman, D.R.: Absorption and Scattering of Light by Small Particles (John Wiley & Sons,)(1983)
- Yoo, K.M., Liu, F., Alfano, R.R.: Phys. Rev. Lett. **64**(22), 2647 (1990). <https://doi.org/10.1103/PhysRevLett.64.2647>
- Fujii, H., Okawa, S., Yamada, Y., Hoshi, Y.: J. Quant. Spectrosc. Radiat. Transf. **147**, 145 (2014). <https://doi.org/10.1016/j.jqsrt.2014.05.026>
- Mishchenko, M.I.: OSA Continuum **1**(1), 243 (2018). <https://doi.org/10.1364/OSAC.1.000243>
- Foldy, L.L.: Phys. Rev. **67**, 107 (1945). <https://doi.org/10.1103/PhysRev.67.107>
- Lax, M.: Phys. Rev. **85**, 621 (1952). <https://doi.org/10.1103/PhysRev.85.621>
- Hunter, R.J.: Foundations of Colloid Science. Oxford University Press Inc., New York (2001)
- Percus, J.K., Yevick, G.J.: Phys. Rev. **110**(1), 1 (1958). <https://doi.org/10.1103/PhysRev.110.1>

48. Fujii, H., Tsang, L., Zhu, J., Nomura, K., Kobayashi, K., Watanabe, M.: *Opt. Express* **28**(15), 22962 (2020). <https://doi.org/10.1364/OE.398582>
49. Baxter, R.J.: *J. Chem. Phys.* **52**(9), 4559 (1970). <https://doi.org/10.1063/1.1673684>
50. Hansen, J.P., McDonald, I.: *Theory of Simple Liquids* (Elsevier,) (2006)
51. Aernouts, B., Van Beers, R., Watté, R., Lammertyn, J., Saeys, W.: *Opt. Express* **22**(5), 6086 (2014). <https://doi.org/10.1364/OE.22.006086>
52. Twersky, V.: *J. Opt. Soc. Am.* **65**(5), 524 (1975). <https://doi.org/10.1364/JOSA.65.000524>
53. Twersky, V.: *J. Acoust. Soc. Am.* **81**, 1609 (1987). <https://doi.org/10.1121/1.394513>
54. Pilvar, A., Smith, D.W., Plutzky, J., Roblyer, D.: *J. Biomed. Opt.* **28**(06), 1 (2023). <https://doi.org/10.1117/1.jbo.28.6.065002>
55. Kodach, V.M., Faber, D.J., Marle, J.V., Leeuwen, T.G.V., Kalkman, J.: *Opt. Express* **19**(7), 6131 (2011). <https://doi.org/10.1364/OE.19.006131>
56. Fujii, H., Terabayashi, I., Aoki, T., Inoue, Y., Na, H., Kobayashi, K., Watanabe, M.: *Appl. Sci.* **12**, 1190–1 (2022). <https://doi.org/10.3390/app12031190>
57. Scheffold, F.: *J. Dispers. Sci. Technol.* **23**(5), 591 (2002). <https://doi.org/10.1081/DIS-120015365>
58. McMillin, R.E., Orsi, D., Cristofolini, L., Ferri, J.K.: *Colloids Interface. Sci. Commun.* **49**, 100641 (2022). <https://doi.org/10.1016/j.colcom.2022.100641>
59. Mason, T.G., Gang, H., Weitz, D.A.: *J. Opt. Soc. Am. A* **14**(1), 139 (1997). <https://doi.org/10.1364/josaa.14.000139>
60. Sutin, J., Zimmerman, B., Tyulmankov, D., Tamborini, D., Wu, K.C., Selb, J., Gulinatti, A., Rech, I., Tosi, A., Boas, D.A., Franceschini, M.A.: *Optica* **3**(9), 1006 (2016). <https://doi.org/10.1364/OPTICA.3.001006>
61. Wang, L.V., Hu, S.: *Science* **335**(6075), 1458 (2012). <https://doi.org/10.1126/science.1216210>
62. Yang, H., Irudayaraj, J.: *LWT - Food Sci. Technol.* **34**(6), 402 (2001). <https://doi.org/10.1006/fstl.2001.0778>
63. Cox, B., Laufer, J.G., Arridge, S.R., Beard, P.C.: *J. Biomed. Opt.* **17**(6), 061202–1 (2012). <https://doi.org/10.1117/1.JBO.17.6.061202>
64. Yao, L., Sun, Y., Jiang, H.: *Phys. Med. Biol.* **55**(7), 1917 (2010). <https://doi.org/10.1088/0031-9155/55/7/009>
65. Brochu, F.M., Brunker, J., Joseph, J., Tomaszewski, M.R., Morscher, S., Bohndiek, S.E.: *IEEE Trans. Med. Imaging* **36**(1), 322 (2017). <https://doi.org/10.1109/TMI.2016.2607199>
66. Okawa, S., Hirasawa, T., Sato, R., Kushibiki, T., Ishihara, M., Teranishi, T.: *Opt. Rev.* **25**(3), 365 (2018). <https://doi.org/10.1007/s10043-018-0435-2>
67. Bench, C., Hauptmann, A., Cox, B.: *J. Biomed. Opt.* **25**(08), 085003–1 (2020). <https://doi.org/10.1117/1.JBO.25.8.085003>
68. Fujii, H., Terabayashi, I., Kobayashi, K., Watanabe, M.: *Photoacoustics* **27**, 100368 (2022). <https://doi.org/10.1016/j.pacs.2022.100368>

**Publisher's Note** Springer Nature remains neutral with regard to jurisdictional claims in published maps and institutional affiliations.